Accepted, August 12, 2009
Preprint typeset using LaTeX style emulateapj v. 04/20/08

arXiv:0908.1621v1 [astro-ph.GA] 12 Aug 2009

DRY MERGERS AND THE FORMATION OF EARLY-TYPE GALAXIES: CONSTRAINTS FROM LENSING AND DYNAMICS

C. Nipoti
Dipartimento di Astronomia, Università di Bologna, via Ranzani 1, 40127 Bologna, Italy

T. Treu
Department of Physics, University of California, Santa Barbara, CA 93106-9530, USA

and

A. S. Bolton
Institute for Astronomy, University of Hawaii, 2680 Woodlawn Dr., Honolulu, HI 96822 USA

Accepted, August 12, 2009

ABSTRACT

Dissipationless (gas-free or "dry") mergers have been suggested to play a major role in the formation and evolution of early-type galaxies, particularly in growing their mass and size without altering their stellar populations. We perform a new test of the dry merger hypothesis by comparing N-body simulations of realistic systems to empirical constraints provided by recent studies of lens early-type galaxies. We find that major and minor dry mergers: i) preserve the nearly isothermal structure ($\rho_{\rm tot} \propto r^{-2}$) of early-type galaxies within the observed scatter; ii) do not change more than the observed scatter the ratio between total mass M and "virial" mass $R_{\rm e}\sigma_{\rm e2}^2/2G$ (where $R_{\rm e}$ is the half-light radius and $\sigma_{\rm e2}$ the projected velocity dispersion); iii) increase strongly galaxy sizes ($R_{\rm e} \propto M^{0.85\pm0.17}$) and weakly velocity dispersions ($\sigma_{\rm e2} \propto M^{0.06\pm0.08}$) with mass, thus moving galaxies away from the local observed M-$R_{\rm e}$ and M-$\sigma_{\rm e2}$ relations; iv) introduce substantial scatter in the M-$R_{\rm e}$ and M-$\sigma_{\rm e2}$ relations. Our findings imply that —unless there is a high degree of fine tuning of the mix of progenitors and types of interactions— present-day massive early-type galaxies cannot have assembled more than $\sim 50\%$ of their mass, and increased their size by more than a factor ~ 1.8, via dry merging.

Subject headings: galaxies: elliptical and lenticular, cD – galaxies: formation – galaxies: kinematics and dynamics – galaxies: structure – gravitational lensing

1. INTRODUCTION

Although early-type galaxies appear to be relatively simple in terms of their internal structure and stellar populations, their formation and evolution are still poorly understood. In the hierarchical model of structure formation, galaxy mergers play a central role in the formation and evolution of early-type galaxies. Many pieces of evidence are consistent with the merging hypothesis (see e.g., van Dokkum 2005, and references therein). However, other observational facts appear hard to reconcile with substantial amounts of merging. Among the facts that have been traditionally used to argue against the central role of mergers are the high observed central density of early-type galaxies (Ostriker 1980; Carlberg 1986); the small scatter in empirical scaling laws such as the color magnitude relation (Bower, Lucey & Ellis 1992), the Fundamental Plane (hereafter FP; Dressler et al. 1987; Djorgovsky & Davis 1987), and the relation between black hole mass $M_{\rm BH}$ and host galaxy mass or central stellar velocity σ_0 dispersion (Ferrarese & Merritt 2000; Gebhardt et al. 2000; Marconi & Hunt 2003; Häring & Rix 2004); and the correlation between abundance ratios and host galaxy properties (e.g., Pipino & Matteucci 2008).

Theoretical and observational studies (e.g., Bender, Burstein & Faber 1992; Ciotti & van Albada 2001; Robertson et al. 2006; Ciotti, Lanzoni & Volonteri 2007; Scarlata et al. 2007; Faber et al. 2007) have argued that a combination of dissipative and dissipationless processes is needed to match the observed properties of early-type galaxies. Dissipation is needed for example to create the high density regions and close to isothermal density profiles, while dissipationless (or "dry") mergers are needed to grow the most massive galaxies while preserving the uniformly old stellar populations and the structural properties of present-day galaxies (e.g. Naab et al. 2007). In particular, both theories and observations have suggested that a large fraction of the immediate progenitors of today's massive red galaxies could be spheroidal galaxies themselves (e.g., van Dokkum et al. 1999; Khochfar & Burkert 2003; Naab, Khochfar, & Burkert 2006; Bell et al. 2006; Faber et al. 2007). Thus, even though mergers may not be the only process at work (e.g., Bundy, Treu & Ellis 2007), dry mergers might play an important role, especially at relatively recent times, i.e. below redshift ~ 1.5, after the bulk of star formation is completed for massive early-type galaxies in the local Universe (e.g., Trager et al. 2000; Treu et al. 2005; Renzini 2006).

In this paper, we take advantage of a new set of constraints provided by strong gravitational lensing studies to test the viability of the dry-merger scenario via a set of numerical simulations. In practice, we first construct realistic models of early-type galaxies so that

Electronic address: carlo.nipoti@unibo.it

they obey known scaling relations between their structural and kinematic properties, and then study how these properties change as a result of dissipationless mergers.

Our approach is similar to that followed by Nipoti, Londrillo & Ciotti (2003a), González-García & van Albada (2003) and Boylan-Kolchin, Ma & Quataert (2006, see also Kazantzidis et al. 2005, Robertson et al. 2006 and Johansson, Naab, & Burkert, 2009a for studies that include dissipation), who tested how the FP, its projections and the $M_{\rm BH}$-σ_0 relation are affected by mergers. The bottom line of these studies is that dry merging between progenitor spheroidal galaxies that lie on the FP, Kormendy (1977) and Faber & Jackson (1976) relations produce spheroidal galaxies that are close to the edge-on FP, but deviate from the Kormendy and Faber-Jackson relations, because they have too large effective radius and too low central velocity dispersion.

Taking a step further, we focus here on lensing-derived properties, testing the results of our simulations against: i) isothermality of the total mass density profile; ii) the correlations between lensing mass and size or stellar velocity dispersion; iii) the Mass Plane, i.e. the correlation between surface mass density, effective radius and velocity dispersion discovered by strong lensing studies. As discussed by Bolton et al. (2007, 2008b), the lensing constraints add a qualitatively new piece of information—an accurate aperture mass for each galaxy—that helps circumvent some of the problems inherent to previous studies. The comparison of N-body simulation with traditional scaling relations is not straightforward, because it relies on assumptions on the mass-to-light ratio to convert luminosity, which enters the observed correlations, into mass. Moreover, among the quantities involved in the traditional empirical correlations (e.g., galaxy luminosity, size, and velocity dispersion), only velocity dispersion is affected by the galaxy dark matter (hereafter DM) content and distribution. Information coming from gravitational lensing, and thus constraining the total galaxy mass distribution, effectively solves this problem.

The paper is organized as follows. First, in § 2 we review the lensing constraints on the structure of early-type galaxies. Then, in § 3, we describe the seed-galaxy models, initial orbital configurations, and numerical methods that we use to simulate the dry-merging process. In § 4 and § 5 we present the results of comparisons between our merger simulations and observations in terms of the effect of dry mergers on density profiles, central DM fractions and scaling relations of galaxies throughout the merging hierarchies. In § 6 we discuss our results in the context of the redshift evolution of early-type galaxies. Finally, § 7 presents our conclusions.

2. LENSING CONSTRAINTS ON THE STRUCTURE OF EARLY-TYPE GALAXIES

The properties of massive early-type galaxies are strongly constrained by the combination of kinematic and strong gravitational lensing observations. In particular, there is growing evidence that these systems have total mass density profile close to isothermal $\rho \propto r^{-2}$ over a large radial interval (Gavazzi et al. 2007), with an intrinsic scatter in logarithmic slope of less than $\sim 10\%$ (Koopmans et al. 2006; Koopmans et al. 2009).

In addition, Bolton et al. (2007, 2008b), using a sample of strong gravitational lenses, have shown that early-type galaxies lie on a Mass Plane (MP)

$$\log R_{\rm e} = a_{\rm m} \log \sigma_{\rm e2} + b_{\rm m} \log \Sigma_{\rm e2} + const, \qquad (1)$$

where $\sigma_{\rm e2}$ is the projected velocity dispersion within an aperture radius $R_{\rm e}/2$ and $\Sigma_{\rm e2}$ is the surface mass density within $R_{\rm e}/2$, with $a_{\rm m} = 1.82 \pm 0.19$, $b_{\rm m} = -1.20 \pm 0.12$ and RMS orthogonal scatter of 1.24 when normalized by the observational errors. The MP is the gravitational lensing analogue of the traditional FP.

The fact that $(a_{\rm m}, b_{\rm m})$ are consistent with $(2, -1)$ and that the scatter is small can be expressed in terms of structural and dynamical homology of the lenses, by

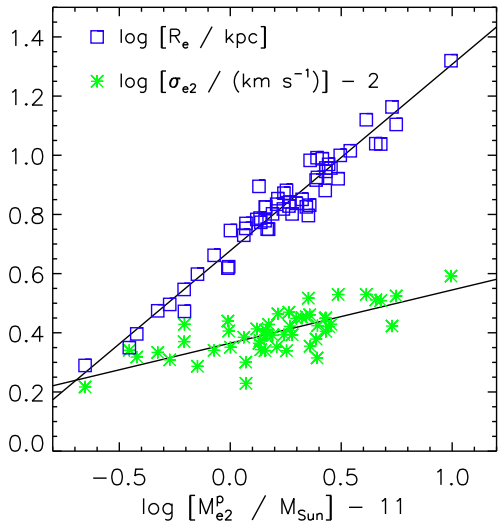

FIG. 1.— Mass-space analogs of the Kormendy and Faber-Jackson relations as defined by data on the SLACS early-type gravitational lens sample from Bolton et al. (2008a). Squares show the variation of half-light radius $R_{\rm e}$ with lensing mass $M^{\rm P}_{\rm e2}$; stars show the variation of velocity dispersion $\sigma_{\rm e2}$ with $M^{\rm P}_{\rm e2}$.

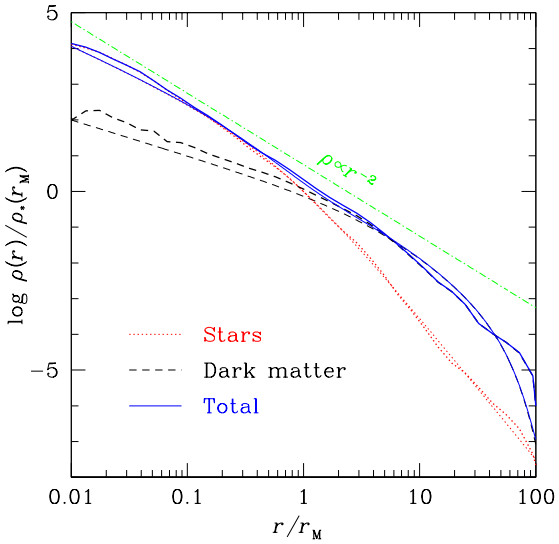

FIG. 2.— Stellar, dark-matter and total density distributions of the seed galaxy (model A; thin curves) and of the end-product (thick curves) of the major-merger simulation 2A5po. $r_{\rm M}$ is the angle-averaged half-mass radius of the stellar distribution.

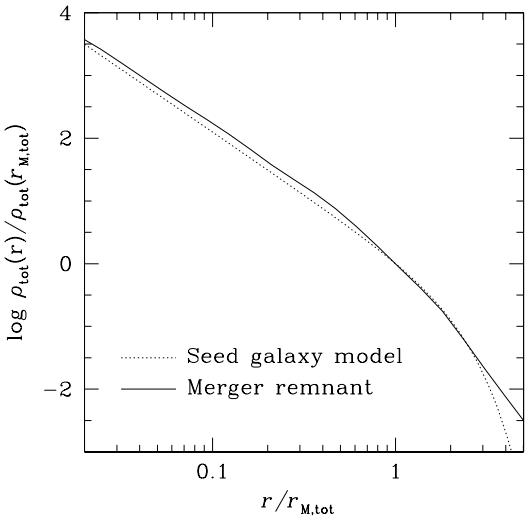

FIG. 3.— Total density profiles of the seed galaxy model (dotted curve) and end-product (solid curve) of a parabolic head-on merging between two identical systems with truncated singular isothermal sphere total density distribution. $r_{\rm M,tot}$ is the angle-averaged half-mass radius of the total mass distribution.

defining the dimensionless structure parameter

$$c_{\rm e2} \equiv \frac{2GM^{\rm p}_{\rm e2}}{R_{\rm e}\sigma^2_{\rm e2}}, \tag{2}$$

where $M^{\rm p}_{\rm e2}$ is the total projected mass within $R_{\rm e}/2$. For their sample of lens early-type galaxies from the Sloan Lens ACS (SLACS) Survey, Bolton et al. (2008b) find on average

$$\langle \log c_{\rm e2} \rangle = 0.53 \pm 0.057. \tag{3}$$

We note that the observed scatter on $\langle \log c_{\rm e2} \rangle$ is 0.08, but here we consider the estimated intrinsic scatter 0.057 (see Bolton et al. 2008b). Importantly, Bolton et al. (2008b) find that $c_{\rm e2}$ has no systematic variation with galaxy mass: this is the sense in which the lens galaxies form a homologous family.

In the present paper we also consider the analogues of the traditional luminosity–size (Kormendy 1977) and luminosity–velocity-dispersion (Faber & Jackson 1976) relations, by deriving the projected-mass–size and the projected-mass–velocity-dispersion relation for the SLACS sample of lenses.

To derive total-mass versions of the Kormendy and Faber-Jackson relations, we use the velocity-dispersion, half-light radius, and lensing-mass measurements for the SLACS strong-lens sample as published in Bolton et al. (2008a). We restrict our attention to the 57 lens systems wherein the lens galaxy has early-type morphology and single multiplicity. For the mass–velocity dispersion relation, we further restrict ourselves to the 53 systems for which the Sloan Digital Sky Survey (SDSS) spectroscopy is of sufficient signal-to-noise to permit a velocity-dispersion measurement. Bolton et al. (2008a) provide lensing measurements using both singular isothermal ellipsoid (SIE) and light-traces-mass (LTM) models for the mass density of the foreground lensing galaxies, which can be used to gauge the dependence of results upon the radial mass-density profile used to extract the strong-lensing aperture masses.

Taking the SIE aperture masses as our reference values, and fitting for the relation that minimizes the orthogonal scatter in logarithmic space, we find a mass–size relationship given by

$$\log\left(\frac{R_{\rm e}}{\rm kpc}\right) = (0.63 \pm 0.02) \times \log\left(\frac{M^{\rm p}_{\rm e2}}{10^{11}M_\odot}\right) + 0.68 \pm 0.01. \tag{4}$$

The observed scatter in $\log R_{\rm e}$ at fixed mass is 0.051, which is reduced to 0.048 by subtracting in quadrature the error in $\log R_{\rm e}$ as estimated by Bolton et al. (2008a) to obtain an estimate of the intrinsic scatter in this quantity. We note that there will be a degree of covariance between the axes of this relation, since the measured $R_{\rm e}$ is used to evaluate the aperture-mass of the SIE model at $R_{\rm e}/2$ to obtain $M^{\rm p}_{\rm e2}$. Fitting similarly for the mass–velocity-dispersion relation, we find

$$\log\left(\frac{\sigma_{\rm e2}}{100\,{\rm km\,s^{-1}}}\right) = (0.18 \pm 0.02) \times \log\left(\frac{M^{\rm p}_{\rm e2}}{10^{11}M_\odot}\right) + 0.36 \pm 0.01. \tag{5}$$

This has an observed scatter in $\log \sigma_{\rm e2}$ at fixed mass of 0.045, implying an intrinsic scatter of 0.034. Errors in all coefficients are computed from the RMS scatter in fits to 1000 bootstrap-resampling draws of 57 or 53 galaxies apiece. Using LTM lensing aperture masses instead of those from SIE models, the coefficients of both relations change only insignificantly. These relations are shown in Fig. 1.

As discussed in several papers (Bolton et al. 2006; Treu et al. 2006; Bolton et al. 2008a; Treu et al. 2009) the SLACS lenses are found to be indistinguishable from control samples of SDSS galaxies with the same stellar velocity dispersion and size, in terms of luminosity/surface brightness, location on the FP, and distribution of environments. We will thus assume that, within the range of observational errors, results found for the lens sample, including the MP, are generic properties of the overall class of massive early-type galaxies.

3. DISSIPATIONLESS MERGING SIMULATIONS

We ran N-body simulations of dissipationless galaxy merging, exploring both major and minor mergers. In the case of major mergers we simulate two colliding systems, which are equal-mass, identical galaxy models with stellar and DM components, and no gas. In major-merger hierarchies, galaxies grow in mass by subsequent binary equal-mass mergers, up to an increase in stellar mass of a factor of ~ 8. In the first step of a hierarchy the seed galaxies are spherically symmetric and non-rotating. In the second step of a hierarchy the end-product of the first step is replicated, and two such galaxies encounter one another. At this stage, the systems are no longer spherically symmetric, thus each of them is initially randomly rotated around its center of mass. The setup of the initial conditions of the third step are obtained in the same way, starting from the remnant of the second step.

In the case of minor mergers, we simulate the accretion of several smaller satellites onto a more massive system (the mass ratio between each satellite and the massive

galaxy is either 1/10 or 1/5). For a galaxy to grow significantly on reasonably short timescales through minor mergers, more than one satellite is expected to interact with the galaxy at the same time. For this reason, we considered hierarchies of minor mergers in which each step is represented by a multiple merger, so the initial conditions represent a massive galaxy surrounded by five or ten infalling satellites. Each galaxy collision is followed up to the virialization of the resulting stellar system. A fraction of the particles is unbound at the end of the simulation: we define the merging end-product as the system composed by the bound stellar and DM particles. We note that in the case of minor-merger hierarchies not all the satellites present in the initial conditions must necessarily merge with the central galaxy. In some cases one or two of the satellites are found on an unbound orbit when all the other systems have already merged and the merger remnant relaxed. When this happens, the satellites are considered escaped and the merging is thus characterized by a significant stellar and DM mass loss.

Altogether we simulated 12 merging hierarchies: 6 major-merger hierarchies of 3 steps each, 2 major-merger hierarchies of 2 steps each, and 4 minor-merger hierarchies of 2 steps each.

3.1. *Seed galaxy models*

The seed galaxy models are spherically symmetric equilibrium two-component systems, with stellar and DM components. The stellar density distribution of the seed galaxies is represented by a γ model (Dehnen 1993; Tremaine et al. 1994):

$$\rho_*(r) = \frac{3-\gamma}{4\pi}\frac{\tilde{M}_*\tilde{r}_*}{r^\gamma(\tilde{r}_*+r)^{4-\gamma}} \qquad (0\leq\gamma<3), \qquad (6)$$

where $\tilde{M}_*$ is the total stellar mass. We assume $\gamma = 1.5$, thus our models are centrally steeper than Hernquist (1990) models ($\gamma = 1$) and shallower than Jaffe (1983) models ($\gamma = 2$). We use $\tilde{r}_*$ and $\tilde{M}_*$ to define time and velocity units $\tilde{t}_* = (\tilde{r}_*^3/G\tilde{M}_*)^{1/2}$ and $\tilde{v}_* = \tilde{r}_*/\tilde{t}_* = (G\tilde{M}_*/\tilde{r}_*)^{1/2}$. The DM halo is described by a Navarro, Frenk & White (1996, NFW) model, so the DM density distribution is

$$\rho_{\rm dm}(r) = \frac{M_{\rm dm,0}}{r(r+r_{\rm s})^2}\exp\left[-\left(\frac{r}{r_{\rm vir}}\right)^2\right], \qquad (7)$$

where $r_{\rm s}$ is the scale radius, $M_{\rm dm,0}$ is a reference mass and we adopt an exponential cut-off to truncate the distribution smoothly at the virial radius $r_{\rm vir}$, so the total DM mass $M_{\rm dm} = 4\pi\int_0^\infty \rho_{\rm dm}(r)r^2dr$ is finite. We assume Osipkov-Merritt (Osipkov 1979; Merritt 1985) anisotropy in the velocity distribution of the stellar component, whose distribution function is then given by

$$f(Q) = \frac{1}{\sqrt{8}\pi^2}\frac{d}{dQ}\int_0^Q \frac{d\varrho_*}{d\Psi_{\rm tot}}\frac{d\Psi_{\rm tot}}{\sqrt{Q-\Psi_{\rm tot}}}, \qquad (8)$$

where

$$\varrho_*(r) = \left(1+\frac{r^2}{r_{\rm a}^2}\right)\rho_*(r). \qquad (9)$$

The variable Q is defined as $Q \equiv \mathcal{E} - L^2/2r_{\rm a}^2$, where the relative (positive) energy is given by $\mathcal{E} = \Psi_{\rm tot} - v^2/2$, v is the modulus of the velocity vector, the relative (positive) total potential is $\Psi_{\rm tot} = \Psi_* + \Psi_{\rm dm}$ (Ψ_* and $\Psi_{\rm dm}$ are, respectively, the relative potentials of the stellar and DM components), L is the angular momentum modulus per unit mass, and $f(Q) = 0$ for $Q \leq 0$. The quantity $r_{\rm a}$ is the so–called anisotropy radius: for $r \gg r_{\rm a}$ the velocity dispersion tensor is mainly radially anisotropic, while for $r \ll r_{\rm a}$ the tensor is nearly isotropic. In the limit $r_{\rm a} \to \infty$, $Q = \mathcal{E}$ and the velocity dispersion tensor becomes globally isotropic.

The orbital distribution of the DM halo is assumed isotropic, so the distribution function of the DM component is given by equation (8) where $Q = \mathcal{E}$ and $\rho_{\rm dm}(r)$ substitutes $\varrho_*(r)$. The total (stars plus DM) density profile is $\rho_{\rm tot}(r) = \rho_{\rm dm}(r) + \rho_*(r)$ and $M_{\rm tot}(r) = 4\pi\int_0^r \rho_{\rm tot}(r')r'^2dr'$ is the total mass within r. This family of $\gamma = 1.5$ plus NFW models have four free parameters: concentration $C_{200} \equiv r_{\rm vir}/r_{\rm s}$, the stellar mass fraction $f_* \equiv \tilde{M}_*/(\tilde{M}_* + M_{\rm dm})$, the ratio $\xi \equiv r_{\rm s}/R_{\rm e}$ and the anisotropy radius $r_{\rm a}$. We consider different choices of these parameters for the seed galaxies of our hierarchies. In what we refer to as model A (see Table 1), we assume $C_{200} = 7$, $f_* = 0.09$, $\xi = 7.8$, so that the resulting total mass profile is close to isothermal ($\rho_{\rm tot} \propto r^{-2}$) in the radial range $0.05 \lesssim r/r_{\rm M} \lesssim 10$ (see thin solid curve in Fig. 2), where $r_{\rm M}$ is the radius of the sphere containing half of the stellar mass, and $r_{\rm a}/\tilde{r}_* = 1.4$, so it lies exactly on the MP ($\log c_{\rm e2} \simeq 0.53$). We also consider models with $C_{200} = 7$, $f_* = 0.09$, $\xi = 7.8$, but different values of $r_{\rm a}/\tilde{r}_*$: an isotropic model ($r_{\rm a}/\tilde{r}_* = \infty$; model B) and a more radially anisotropic model ($r_{\rm a}/\tilde{r}_* = 0.7$; model C). In other hierarchies the seed galaxy is more DM dominated (model D): a $\gamma = 1.5$ plus NFW model with $C_{200} = 8$, $f_* = 0.02$, $\xi = 11.6$ and $r_{\rm a}/\tilde{r}_* = 1$ so that also this model has close-to-isothermal total density profile and has $\log c_{\rm e2} \simeq 0.53$.

Our seed galaxy models are primarily constructed to reproduce the total density distribution and structural parameter $c_{\rm e2}$ of massive ($M_* \sim 10^{11}M_\odot$) local early-type galaxies, as constrained by strong gravitational lensing and kinematics; we did not attempt a full exploration of the space of parameters C_{200}, f_* and ξ, but we adopted values that are expected to bracket the ranges expected on the basis of theoretical investigations (see Nipoti, Treu & Bolton 2008, and references therein). Additional observational constraints on the DM content of present-day early-type galaxies come from weak gravitational lensing surveys (Mandelbaum et al. 2006; Gavazzi et al. 2007). According to the weak-lensing results of Mandelbaum et al. (2006) the stellar mass fraction f_* of $M_* \sim 10^{11}M_\odot$ early-type galaxies are of the order of $0.03 - 0.06$ (if uncertainties on the Initial Mass Function are taken into account), so the values of f_* of our seed galaxy models bracket the observationally estimated range of f_* for systems of this mass. However, f_* estimated from weak-lensing tend to decrease with stellar mass above $M_* \sim 10^{11}M_\odot$ (Mandelbaum et al. 2006), so the more DM dominated model D ($f_* = 0.02$) should be considered more realistic than model A to represent more massive systems.

To address the question of whether r^{-2} density profiles are preserved by merging we also ran an equal-mass merger simulation in which each seed galaxy is a one-

component system with total density profile

$$\rho_{\rm tot}(r) = \rho_{\rm tot,0} \left(\frac{r_{\rm t}}{r}\right)^2 \exp\left[-\left(\frac{r}{r_{\rm t}}\right)^2\right], \qquad (10)$$

where $\rho_{\rm tot,0}$ is a reference density. The density distribution in the equation above is that of a singular isothermal sphere (SIS), smoothly truncated at a radius $r_{\rm t}$ so that the total mass $M_{\rm tot} = 4\pi \int_0^\infty \rho_{\rm tot}(r) r^2 dr$ is finite. This truncated SIS model is assumed isotropic.

3.2. *Major-merging simulations*

In the case of major-merging hierarchies, in each step we follow the evolution of a binary galaxy encounter, characterized by the properties of the colliding systems and of their mutual orbit, which we parametrize with the standard two-body approximation. For an encounter between two galaxies of total masses M_1 and M_2 we define the orbital energy per unit mass

$$E = \frac{1}{2} v_0^2 - \frac{G(M_1 + M_2)}{d_0}, \qquad (11)$$

and the orbital angular momentum per unit mass $\mathbf{L} = \mathbf{d}_0 \times \mathbf{v}_0$, where $\mathbf{d}_0$ and $\mathbf{v}_0$ are the relative separation and velocity vectors of the centers of mass of the two colliding systems at the initial time of the simulation. We ran simulations of parabolic ($E = 0$), elliptic ($E < 0$) and hyperbolic ($E > 0$) orbits, and we explored both head-on encounters ($L = 0$) and off-center encounters ($L > 0$). In the case of encounters between two equal-mass, identical galaxies it is useful to define the dimensionless orbital energy $\hat{E} \equiv 2E/\sigma_{\rm v}^2$ and angular momentum modulus $\hat{L} \equiv L/\sigma_{\rm v} r_{\rm M,tot}$, where $\sigma_{\rm v}$ is the virial velocity dispersion and $r_{\rm M,tot}$ is the angle-averaged half-mass radius of the total density distribution of the isolated systems (Binney & Tremaine 1987). We consider six different major merging hierarchies, with seed galaxy model A, in which the orbital parameters $\hat{E}$ and $\hat{L}$ are the same in each step of the hierarchy. Only in the last step (run 8A1ho) of the off-center hyperbolic major-merger hierarchy $\hat{E}$ and $\hat{L}$ are smaller than in the previous steps, in order to avoid a too long merging timescale. In addition we explore two parabolic hierarchies having as seed galaxy model D (one with $L = 0$, the other with $L > 0$). The parameters of the simulations are summarized in Tables 1 and 2.

3.3. *Minor-merging simulations*

We present four minor-merging hierarchies, each consisting of two steps of (multiple) minor-merging simulations. Let us focus first on the hierarchy represented by the two simulations 2A1m10x and 4A1m10x: in the first step of this hierarchy the initial conditions consist of a central galaxy model A, of stellar mass $\tilde{M}_*$ and scale radius $\tilde{r}_*$, surrounded by ten identical satellites, also represented by model A, but with stellar mass $\tilde{M}_*/10$ and scale radius $0.23\tilde{r}_*$. The satellites are randomly distributed around the central galaxy with relative distance between each satellite and the central galaxy in the range $100 - 140\,\tilde{r}_*$ and with velocity directed towards the center of mass of the central galaxy. The relative speed between each satellite and the central galaxy is such that the orbit would be parabolic in the absence of the other satellites. The end-product of run 2A1m10x is used as central galaxy of the initial conditions in the second step of the hierarchy, in which it is surrounded by ten identical satellites of mass $\tilde{M}_*/5$ and scale radius $0.36\tilde{r}_*$ with distribution analogous to run 2A1m10x, but now with relative distance with respect to the central galaxy in the range $200 - 280\,\tilde{r}_*$. Though each satellite would be on a radial parabolic orbit in the absence of the other satellites, the latter act as perturbers, so the orbits are actually neither strictly radial nor strictly parabolic.

The set-up of the other minor-merging hierarchies are similar to the one described above. The hierarchy (2A1m10y, 4A1m10y) is just another realization of the same set-up: the initial conditions differ just in the relative distribution in phase space of the centers of mass of the satellites. In the hierarchy (2A1m5, 4A1m5) we adopt five satellites per step instead of ten, with stellar mass $0.2\tilde{M}_*$ ($0.4\tilde{M}_*$) and scale radius $0.36\tilde{r}_*$ ($0.56\tilde{r}_*$) in the first (second) step. In the hierarchy (2D1m10, 4D1m10) the initial central galaxy and the ten satellites are represented by model D, with same scale radii and masses as (2A1m10x, 4A1m10x), but relative distance between each satellite and the central galaxy in the range $170 - 230\,\tilde{r}_*$ (first step) and $340 - 460\,\tilde{r}_*$ (second step), on account of the more extended DM distributions.

3.4. *Numerical methods*

For the simulations we used the parallel N-body code FVFPS (Fortran Version of a Fast Poisson Solver; Londrillo, Nipoti, Ciotti 2003; Nipoti, Londrillo & Ciotti 2003a), based on Dehnen (2002) scheme. We adopt the following values for the code parameters: minimum value of the opening parameter $\theta_{\rm min} = 0.5$ and softening parameter $\varepsilon = 0.03 - 0.1$ in units of $\tilde{r}_*$ (depending on the number of particles and on the size of the merging systems). The time-step Δt, which is the same for all particles, is allowed to vary adaptively in time as a function of the maximum particle density $\rho_{\rm max}$: in particular, we adopted $\Delta t = 0.3/(4\pi G \rho_{\rm max})^{1/2}$.

Numerically, the initial distribution of the seed galaxy particles in phase space is realized as described in Nipoti, Londrillo & Ciotti (2002). While the gravitational potential Ψ_* is analytic, $\Psi_{\rm dm}$ is computed by numerical integration, given the spherically symmetric density distribution (7). We verified that the seed galaxy models are in equilibrium by evolving them in isolation for several dynamical times. As a rule, in the first step of each merging hierarchy we use $N_* \simeq 4 \times 10^4$ stellar particles and $N_{\rm dm} \simeq 4 \times 10^5$ (when $f_* = 0.09$) or $N_{\rm dm} \simeq 2 \times 10^6$ (when $f_* = 0.02$; halo and stellar particles have the same mass). Clearly, the number of particles increases with the hierarchy steps, up to $N_{\rm tot} = N_{\rm dm} + N_* \simeq 1.7 - 3.9 \times 10^6$ in the last steps considered.

The intrinsic and projected properties of the merger remnants are determined following Nipoti, Londrillo & Ciotti (2002, 2006). In particular, we measure the axis ratios c/a and b/a of the inertia ellipsoid (where a, b and c are the major, intermediate and minor axis), and the angle-averaged density distribution of the stellar and DM components.

We also measure the angle-averaged half-mass radius of the stellar density distribution ($r_{\rm M}$) and of the total density distribution ($r_{\rm M,tot}$). For each end-product, in order to estimate the importance of projection effects, we consider 50 random projections and we use them to compute average projected quantities and associated 1-σ scatter. For each projection we measure the ellipticity $\epsilon = 1 - b_{\rm e}/a_{\rm e}$, the circularized projected density profile and the circularized effective radius $R_{\rm e} \equiv \sqrt{a_{\rm e} b_{\rm e}}$ (where $a_{\rm e}$ and $b_{\rm e}$ are the major and minor semi-axis of the effective isodensity ellipse). In addition, we measure the central projected velocity dispersion $\sigma_{\rm e2}$, obtained by averaging the projected velocity dispersion over the circularized surface density profile within an aperture of $R_{\rm e}/2$. The projected mass $M^{\rm p}_{\rm e2}$ is computed by counting stellar and DM particles within the same projected elliptical aperture with circularized radius $R_{\rm e}/2$.

As a convergence test, we reran three of the simulations at higher resolution (with five times more particles), finding good agreement with the lower-resolution cases. In particular, the runs 2A5ph, 2A5po and 2A5m10x differ from the runs 2A1ph, 2A1po and 2A1m10x, respectively, just for the number of particles of the seed galaxies (see Tables 1 and 2): the quantities $R_{\rm e}$, $\sigma_{\rm e2}$ and $M^{\rm p}_{\rm e2}$, which are crucial for the present study, are indistinguishable in lower and higher resolution simulations.

4. EFFECT OF DRY MERGERS ON THE MASS DENSITY DISTRIBUTION

4.1. *Total density profiles*

From lensing studies we know that the total density profiles of early-type galaxies are close to isothermal over a large radial range. Here we address the question of whether such a feature is preserved by dry major and minor merging. As a first experiment we consider the merging between two identical truncated SISs with total density distribution (10). In this simple case each seed galaxy model is one-component, so we do not distinguish between DM and baryons. Figure 3 plots the total density profiles of the seed models and of the merger remnant of this run. By construction, the seed model has density profile $\propto r^{-2}$ within $\sim r_{\rm M,tot}$ and steeper at larger radii because of the exponential truncation. The density profile of the merging end-product is very similar to that of the seed galaxy: fitting it with a power law $r^{-\gamma'}$ in the radial range $0.03 < r/r_{\rm M,tot} < 1$ we get a best-fitting index $\gamma' = 2.00 \pm 0.01$. The finding that the *inner* density cusp is preserved by dissipationless merging is consistent with theoretical expectations (Dehnen 2005) and previous numerical experiments (Fulton & Barnes 2001; Kazantzidis, Zentner & Kravtsov 2006). Our simulation shows that *the $\sim r^{-2}$ density profile is preserved by dry major merging not only in the central regions, but throughout the system.*

Let us now consider how the total density profile is affected by merging more realistic (two-component) stellar systems. Figure 4 plots, as a function of radius, the (angle-averaged) total density distributions of our six reference major merging hierarchies, having as seed galaxy model A and differing for the orbital parameters of the galaxy encounters. From the diagrams it is apparent that the merging process affects significantly the *normalization* of the density profile (producing systems of lower density at the half-light radius; see also § 5), but it roughly preserves its *shape*. To quantify the effect of dry merging on the shape of the total mass density distribution we fit the total intrinsic density profiles of our models with a power law $r^{-\gamma'}$ over the radial range $0.1 \lesssim r/R_{\rm e} \lesssim 1$, where $R_{\rm e}$ is the average of the circularized half-light radius over 50 random projections. By construction our seed galaxy models have close-to-isothermal total density profile: in the radial range $0.1 \lesssim r/R_{\rm e} \lesssim 1$ model A and model D are best fitted with $\gamma' = 2.02 \pm 0.02$ and $\gamma' = 2.00 \pm 0.01$, respectively. Figure 5 shows the distribution of the best-fitting γ' for the end-products of all steps of our merging hierarchies (30 steps altogether). It is apparent that dry merging can make slightly steeper or shallower the total density profile, depending on the characteristics of the galaxy encounters. The distribution has mean $\langle\gamma'\rangle \simeq 2.01$ and standard deviation $\sigma_{\gamma'} \simeq 0.18$ ($\sim 9\%$). This is comparable with the observationally determined values $\langle\gamma'\rangle \simeq 2.08 \pm 0.1$ and standard deviation $\sigma_{\gamma'} \lesssim 0.20$ (Koopmans et al. 2009), suggesting that if a population of early-type galaxies has initially close-to-isothermal total density profile, dry merging tends to maintain this property, but adds non-negligible scatter.

The best-fitting values of γ' for the single simulations are reported in Table 2 together with the other simulation parameters: off-axis major mergers tend to produce steeper density profiles than head-on encounters, while there is no evidence of a dependence of γ' on the orbital energy. Minor and major merging involving more DM dominated galaxies (model D) tend to decrease γ'.

We focused on the slope of the total density profile over the radial range $0.1 \lesssim r/R_{\rm e} \lesssim 1$, which is approximately the range probed in combined strong-lensing and stellar kinematics observations. However, we note that the total density profiles of our seed models and merger remnants are well represented by a power-law over a much larger radial range, though the power-law index is rather sensitive to the radial interval. For instance, seed models A and D are fitted over the larger radial range[1] $0.1 \lesssim r/R_{\rm e} \lesssim 10$ with $\gamma' = 2.17 \pm 0.02$ and $\gamma' = 1.94 \pm 0.02$, respectively. Also fitting over this larger radial range, the end-products are found to have slightly larger or smaller best-fitting γ' than the seed galaxy of their hierarchy.

4.2. *Central dark-matter fractions*

We have seen that dry merging tends to preserve the slope of the total density profile. We also found that the shape of the density distributions of stars and DM is not dramatically affected by dry mergers (see Fig. 2), though there is redistribution between DM and stars that leads to a systematic increase with merging of the projected DM-to-total mass ratio $f^{\rm p}_{\rm dm}$ within $R_{\rm e}$. This is apparent from the upper panel Fig. 6, plotting $f^{\rm p}_{\rm dm}(R < R_{\rm e})$ as a function of M_* for our major and minor merging hierarchies. The seed galaxy models have $f^{\rm p}_{\rm dm} = 0.25$ (model A) and $f^{\rm p}_{\rm dm} = 0.45$ (model D), while the merger remnants have DM fractions in the range $0.3 \lesssim f^{\rm p}_{\rm dm} \lesssim 0.7$. In all cases $f^{\rm p}_{\rm dm}$ increases with the stellar mass along the merging hierarchy. Taken by itself this effect might

[1] Larger radial ranges are interesting for comparison with weak-lensing observations of early-type galaxies (Gavazzi et al. 2007).

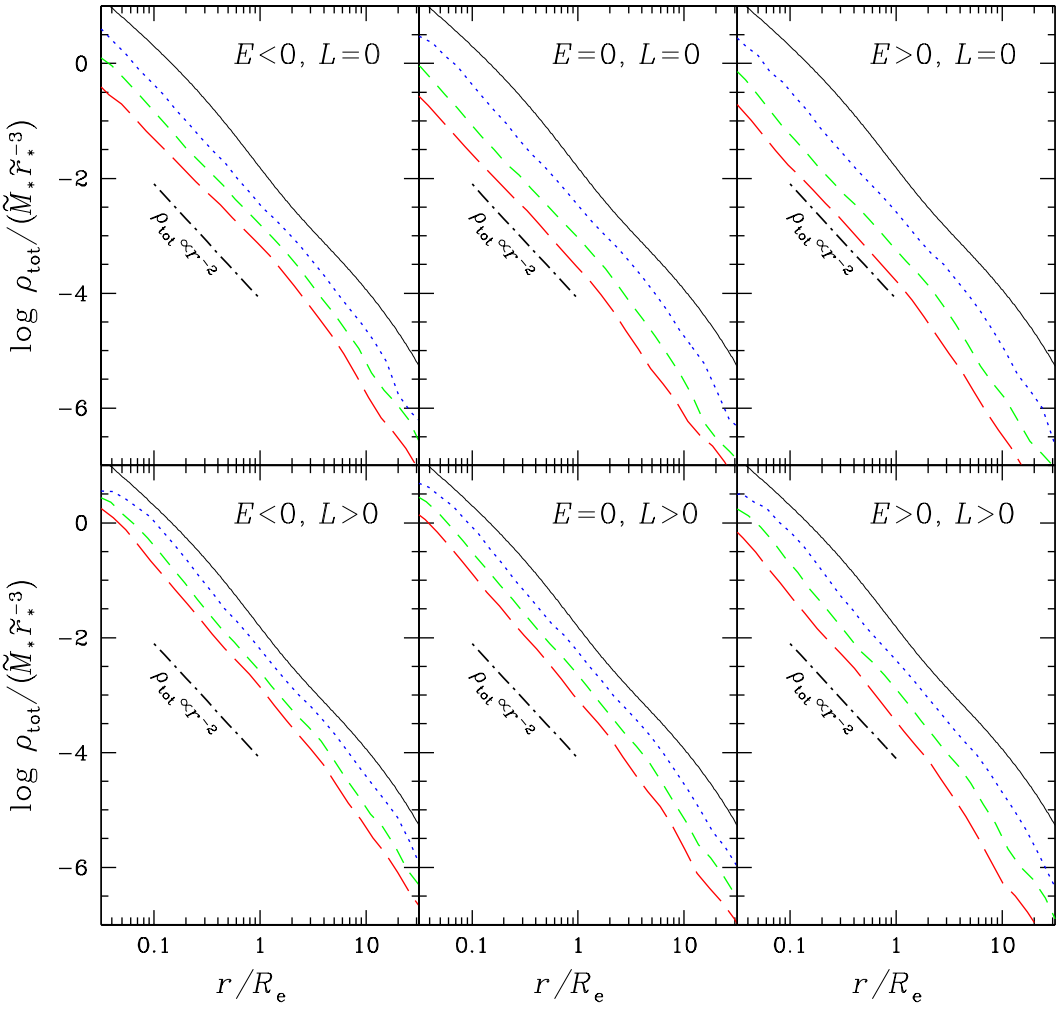

FIG. 4.— Total density distributions of the seed galaxy (solid curves) and of the end-products of six major-merging hierarchies having the same seed galaxy (model A), but different orbital parameters. $R_{\rm e}$ is the average of the effective radius over 50 random lines of sight. The end-products of the first, second and third steps of the hierarchies are represented by dotted, short-dashed and long-dashed curves, respectively. The dash-dotted line represents the isothermal distribution ($\rho_{\rm tot} \propto r^{-2}$) in the radial range $0.1 \leq r/R_{\rm e} \leq 1$, over which we fit the profiles.

be interpreted as quite naturally explaining the "tilt" seen in the luminosity-based FP relation in terms of a systematic increase in the central DM fraction with increasing mass. If more luminous and massive galaxies represent a later stage in the merging hierarchy, this increased central DM fraction will lead to a larger dynamical mass per unit luminosity as compared to less massive (and less merged) galaxies. However, the increase of $f_{\rm dm}^{\rm p}(R < R_{\rm e})$ with mass during the merging hierarchy is mainly driven by a strong increase in the effective radius produced by dry merging, which might be considered an argument against the relevance of dry mergers in the assembly of elliptical galaxies (see § 5). In fact, the trend is quite different if one considers $f_{\rm dm}^{\rm p}$ as measured within a small aperture of fixed radius, independent of the galaxy's half-light radius. For instance, in the lower panel of Fig. 6 we show the results obtained by measuring the projected DM fraction within and aperture of radius $R = \tilde{r}_*$. We note that $\tilde{r}_*$ ranges from $\simeq 0.8R_{\rm e}$ for the seed galaxies, to $\tilde{r}_* \simeq 0.07R_{\rm e}$ for the most extended remnant. We find that the remnants have $f_{\rm dm}^{\rm p}(R < \tilde{r}_*)$ close the value measured in the seed galaxy of their hierarchy, indicating that the central projected DM fraction, measured within a region of fixed size in physical units, is not substantially affected by dry merging. Interestingly, minor mergers (stars, diamonds and crosses in the diagrams) tend to produce systems with higher values of $f_{\rm dm}^{\rm p}$ than major mergers (circles and squares in the diagrams), indicating that dynamical-friction heating (El-Zant et al. 2004; Nipoti et al. 2004; Romano-Díaz et al. 2008; Johansson, Naab, & Ostriker 2009b) is effectively balanced by accretion of DM in the central regions (see Nipoti et al. 2004, for a discussion).

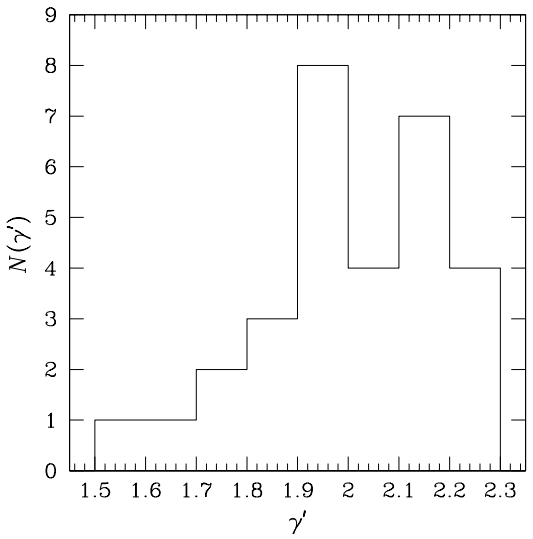

FIG. 5.— Distribution of the values of the best-fit power-law index of the total density distribution $\rho_{\rm tot} \propto r^{-\gamma'}$ for the end-products of all steps of minor and major merging hierarchies. The distribution has mean $\langle\gamma'\rangle \simeq 2.01$ and standard deviation $\sigma_{\gamma'} \simeq 0.18$.

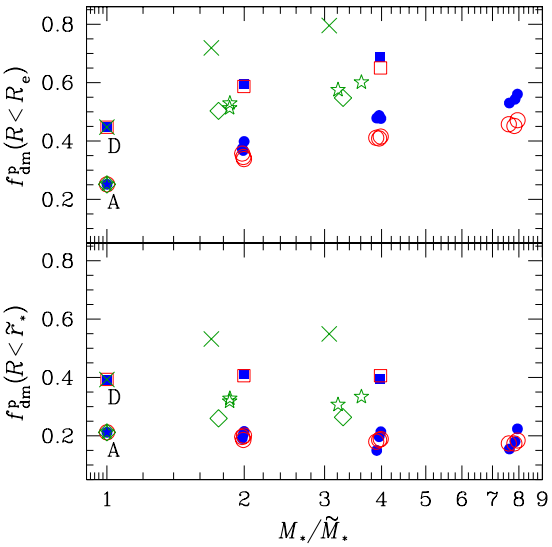

FIG. 6.— Upper panel: projected dark-matter-to-total-matter mass ratio within $R_{\rm e}$ as a function of the stellar mass for the major (circles and squares) and minor (stars, diamonds and crosses) merging hierarchies. The points representing the seed ($M_*/\tilde{M}_* = 1$) galaxy models A and D are labelled. For the merger remnants $f^{\rm p}_{\rm dm}$ depends on the line of sight, but projection effects are small, so just the average value is plotted. Lower panel: same as upper panel, but plotting projected dark-matter-to-total-matter mass ratio within an aperture of radius $R = \tilde{r}_*$ (same radius, in physical units, for all models).

5. EFFECT OF DRY MERGERS ON THE LENSING SCALING RELATIONS

We address here the question of whether the lensing scaling relations are preserved by major and minor dry merging. For this reason we consider seed galaxy models that lie on the observed correlations and we investigate whether the merger remnants are consistent with the same relations within their intrinsic scatter. Nipoti, Londrillo & Ciotti (2003a) pointed out that, when comparing merging simulations with the standard (luminosity based) scaling relations of early-type galaxies, it is crucial to consider not only the edge-on FP, but also the Faber-Jackson and the Kormendy relation, because a system may well lie on the FP while deviating significantly from the other relations. Similarly, the fact that a galaxy model lies on the MP does not mean that it satisfies also the the observed lensing mass-size and mass-velocity dispersion relations, because —for fixed $M^{\rm p}_{\rm e2}$— anomalous values of both $\sigma_{\rm e2}$ and $R_{\rm e}$ can conspire to give a value of $c_{\rm e2}$ perfectly consistent with observations. For this reason we will study how our merger hierarchies behave with respect to all three lensing scaling laws.

5.1. *Placing the seed galaxies on the observed scaling relations*

As discussed extensively in Nipoti, Treu & Bolton (2008), for a spherical galaxy model the dimensionless quantity $c_{\rm e2}$ is fully determined by the stellar and DM density profiles, and by the distribution of the orbital velocity of stars. Of course, purely dynamical systems such as our seed galaxy models can be rescaled arbitrarily by choosing their mass scale $\tilde{M}_*$ and length scale $\tilde{r}_*$ in physical units. While the value of $c_{\rm e2}$ is independent of this choice, in order to place a model on the observed mass-size and mass-velocity dispersion relations, mass and length scales must be chosen consistently.

Given that the MP relation has no tilt and that the observed mass-size and mass-velocity dispersion relations are consistent with power laws over the range covered by the lensing data (equations [1], [4] and [5]), we would not need to specify the mass of the seed galaxy in order to address the question of the effect of dry merging. It is sufficient to check whether the merging end-products have values $c_{\rm e2}$ consistent with the MP and the relative change of $M^{\rm p}_{\rm e2}$, $R_{\rm e}$ and $\sigma_{\rm e2}$ are consistent with the observed mass-size and mass-velocity dispersion relations. However, just for clarity and without loss of generality, we fix $\tilde{M}_* = 10^{11} M_\odot$, so all our seed galaxies have total stellar mass $M_* = 10^{11} M_\odot$. The projected mass $M^{\rm p}_{\rm e2} = 3.73 \times 10^{10} M_\odot$ for galaxy model A and $M^{\rm p}_{\rm e2} = 4.48 \times 10^{10} M_\odot$ for galaxy model D. We then fix $\tilde{r}_* = 2.08$ kpc for model A and $\tilde{r}_* = 2.34$ kpc for model D, so that they lie on the $M^{\rm p}_{\rm e2} - R_{\rm e}$ relation (and, as a consequence, on the $M^{\rm p}_{\rm e2} - \sigma_{\rm e2}$ relation, because they lie on the MP by construction). The satellites in the minor-merger hierarchies have masses and characteristic radii proportionally smaller than those of the central galaxy (see § 3.3), but such that they also satisfy the scaling laws. Clearly, $\tilde{M}_*$ and $\tilde{r}_*$ are kept fixed throughout each hierarchy, so masses, sizes and velocities of all remnants are now known in physical units.

5.2. *Comparing the merger remnants with the observed scaling relations*

The location of the merger remnants with respect to the observed scaling laws is shown in Figs. 7, 8 and 9. We note that the total projected mass $M^{\rm p}_{\rm e2}$ within $R_{\rm e}/2$ increases with dry merging more than the stellar mass or the total mass integrated over the entire system. This can be seen, for instance, in Fig. 7: in three merging steps $M^{\rm p}_{\rm e2}$ increases by more than a factor of ten, while the stellar or total mass, integrated over the entire system, can increase at most by a factor of eight (in fact

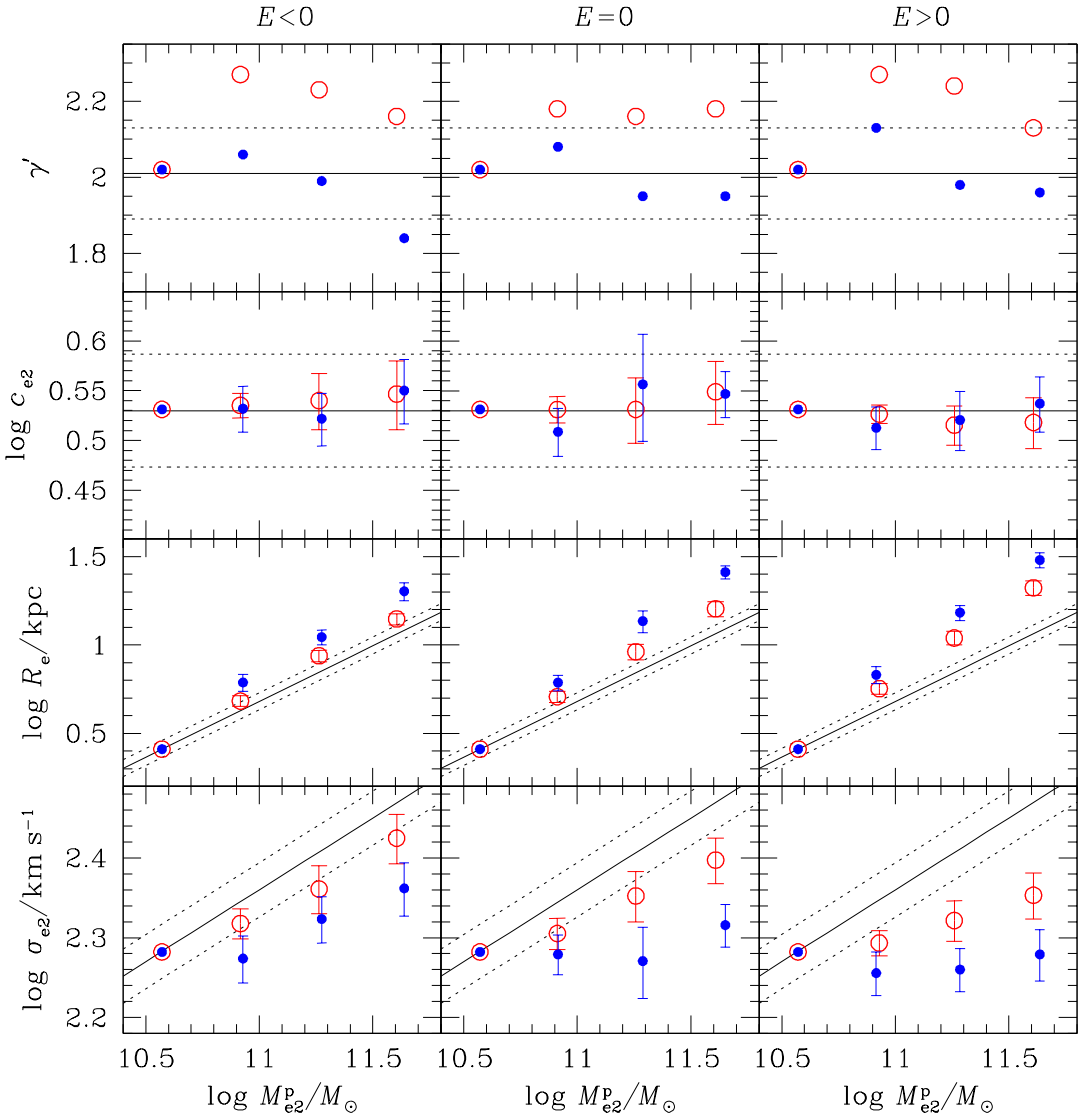

FIG. 7.— From top to bottom: best-fitting logarithmic slope γ' ($\rho_{\rm tot} \propto r^{-\gamma'}$) of the total density profile (first row), structure parameter $c_{\rm e2}$ (second row), effective radius (third row) and projected velocity dispersion $\sigma_{\rm e2}$ (fourth row), as functions of the projected mass $M^{\rm P}_{\rm e2}$, for elliptic (left column), parabolic (central column) and hyperbolic (right column) major-merging hierarchies with seed galaxy model A. Points and error bars represent the average value and the 1-σ scatter (due to projection effects) for simulated galaxies: filled circles are for head-on encounters and empty circles for off-axis encounters. $M^{\rm P}_{\rm e2}$ depends on the line-of-sight, but error bars are smaller than the symbol size, so they are not plotted. Solid and dotted lines represent the observed correlations with 1-σ scatter.

less, as a consequence of mass loss). This finding indicates that dry merging redistributes matter so that the fraction of mass found in a cylinder of radius $R_{\rm e}/2$ increases significantly.

Let us focus now on the behavior of the merger hierarchies with respect to the MP, which is illustrated in the second row of panels of Fig. 7, 8 and 9. In general, the intermediate and final remnants of all our merger hierarchies are found to be very close to the MP. Actually, all the remnants of model-A merging hierarchies have values of $c_{\rm e2}$ within the observed scatter of the MP, while the end-products of the model-D merger hierarchies (squares and crosses in Fig. 8) have slightly higher values of $c_{\rm e2}$, and are only marginally consistent with the MP. This result implies that $c_{\rm e2}$ is a robust parameter, since its value is essentially preserved under a wide range of dry-merging histories. In a scenario in which early-type galaxies grow significantly by dry merging, the characteristic value of $c_{\rm e2}$ must therefore be established by the dissipative ("wet") formation processes of the primordial progenitor galaxies. The implications of the observed value of $c_{\rm e2}$ for galaxy *structure* (as opposed to evolution) are the subject of Nipoti, Treu & Bolton (2008). Remarkably, dry merging appears also to wash out the effect of orbital anisotropy on $c_{\rm e2}$: the end-products of mergers whose seed galaxies differ only in the velocity distribution of their stars (and thus have different values of $c_{\rm e2}$; see Nipoti, Treu & Bolton 2008) are indistinguishable in the space of the parameters $M^{\rm P}_{\rm e2}$, $R_{\rm e}$ and $\sigma_{\rm e2}$ (see Fig. 9).

As anticipated above, the fact the MP is "closed" with respect to dry merging does not mean that

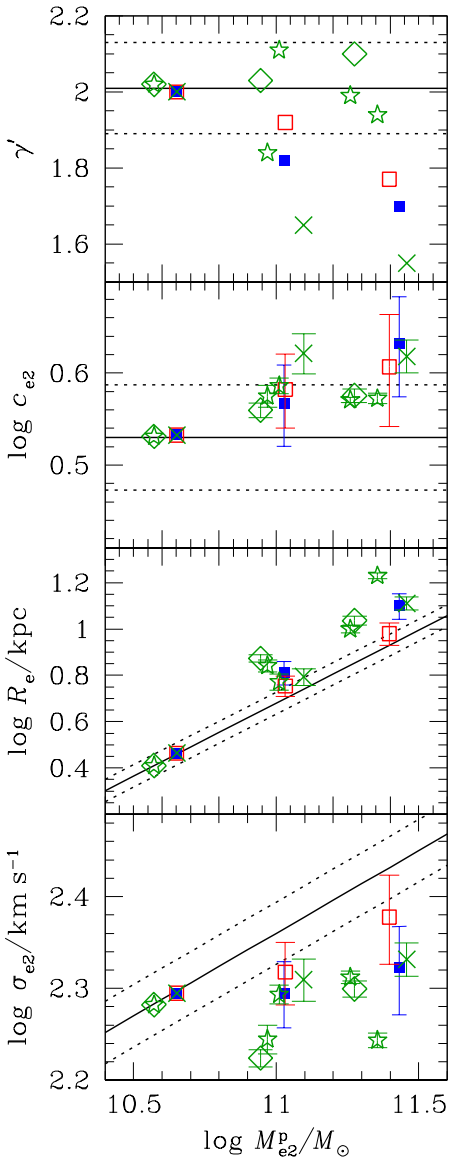

FIG. 8.— Same as Fig. 7, but for parabolic major-merger hierarchies having as seed galaxy model D (solid squares are for head-on encounters and empty squares for off-axis encounters), and for the following minor merging hierarchies: model-A hierarchies with ten satellites per step (stars) and five satellites per step (diamonds), and the model-D hierarchy with ten satellites per step (crosses).

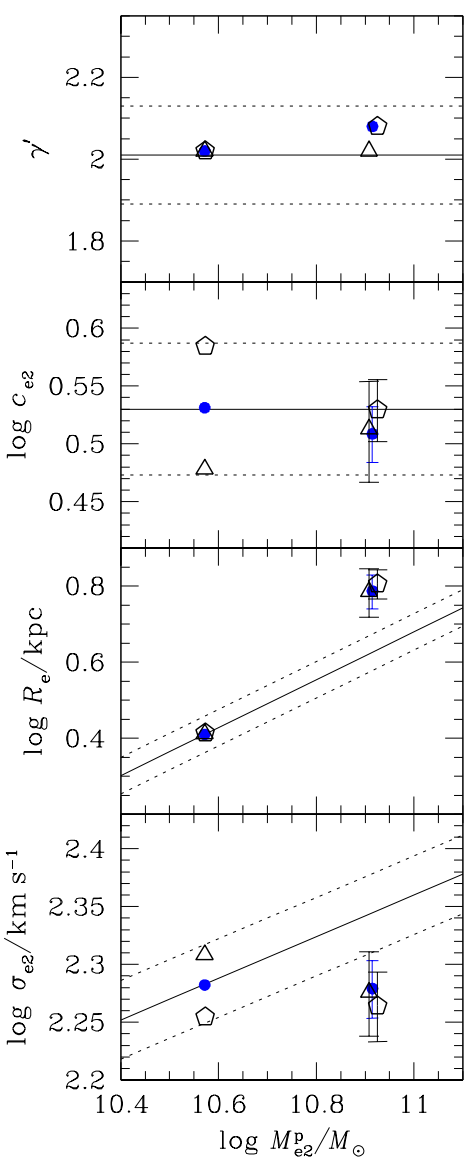

FIG. 9.— Same as Fig. 7, but for the seed models and end-products of three head-on parabolic major-merging simulations differing only for the anisotropy of their seed galaxy models: 2A5ph (circles; $r_a/\tilde{r}_* = 1.4$), 2B5ph (triangles; $r_a/\tilde{r}_* = \infty$) and 2C5ph (pentagons, $r_a/\tilde{r}_* = 0.7$).

the same must be true also for the mass–velocity-dispersion and mass–size relations. In fact, as might be expected from previous explorations of the effect of dry merging on the Faber-Jackson and Kormendy relations (Nipoti, Londrillo & Ciotti 2003a; Boylan-Kolchin, Ma & Quataert 2006), the end-products of all the merger hierarchies are found to deviate significantly from the M^p_{e2}-R_e and M^p_{e2}-σ_{e2} relations, because they have too large R_e and too low σ_{e2} for their mass (see third and fourth rows of panels in Fig. 7, 8 and 9). It turns out that the too large R_e and too low σ_{e2} compensate, giving values of c_{e2} very close to the observed one (we recall that R_e and σ_{e2} appear in the definition of c_{e2} just in the product $R_e\sigma^2_{e2}$; see equation [2]). Some of the minor-merger hierarchies lead to strong deviations from the observed scaling relations (see right-most stars in Fig. 8): in some steps R_e increases with M^p_{e2} more than linearly, and σ_{e2} decreases with M^p_{e2}, consistent with recent results by Naab, Johansson, & Ostriker (2009). In other cases the increase in size is significantly smaller, suggesting that the structural effect of minor merging is quite dependent on the details of the interaction, such as DM distribution and orbits of the satellites. In the merging hierarchies having as seed galaxy model D, whose end-products are found slightly off the MP, the deviations from the mass-size and mass-velocity dispersion relation are in general relatively small (squares and crosses in Fig. 8), and marginally consistent with the observed relations in the case of off-axis major mergers (open squares in Fig. 8). In these cases low values of σ_{e2} are not compensated by large enough R_e.

In the top panels of Fig. 7, 8 and 9 the total-density

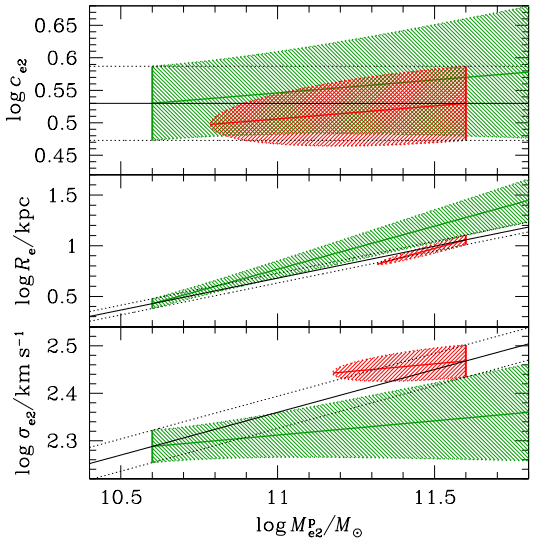

FIG. 10.— Top: the green shaded area represents the expected distribution, within 1 σ, of the merger remnants of a population of galaxies all with the same projected mass $M^{\rm p}_{\rm e2} = 10^{10.6} M_\odot$, and a distribution of $c_{\rm e2}$ matching the observed one (see § 5). The red shaded area represents the location in the $M^{\rm p}_{\rm e2} - c_{\rm e2}$ plane of possible dry-merging progenitors of a $z = 0$ early-type galaxy with projected mass $M^{\rm p}_{\rm e2} = 10^{11.6} M_\odot$ (see § 6). Central and bottom panels: same as top panel, but in the $M^{\rm p}_{\rm e2} - R_{\rm e}$ and $M^{\rm p}_{\rm e2} - \sigma_{\rm e2}$ planes. Symbols are the same as in Figs. 7 and 8. Solid and dotted lines represent the observed correlations with 1-σ scatter.

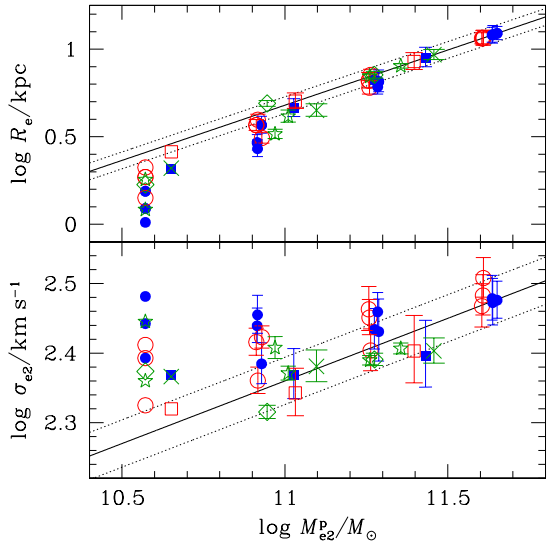

FIG. 11.— Effective radius (upper panel) and projected velocity dispersion (lower panel) of the seed galaxies and merger remnants of all steps of our major and minor merging hierarchies. For each hierarchy, $\tilde{M}_*$ and $\tilde{r}_*$ are set so that the remnant of the last step lies on the local $M^{\rm p}_{\rm e2} - R_{\rm e}$ relation. Solid and dotted black lines represent the local observed correlations with 1-σ scatter. Symbols are the same as in Fig. 7 and 8.

slope γ' (see § 4) is plotted as a function of mass for the seed galaxies and the remnants. The behavior on the $M^{\rm p}_{\rm e2}$-γ' plane is not strictly correlated to that in the $M^{\rm p}_{\rm e2}$-$c_{\rm e2}$, $M^{\rm p}_{\rm e2}$-$R_{\rm e}$ and $M^{\rm p}_{\rm e2}$-$\sigma_{\rm e2}$ planes, though we note that models that deviate more from the $M^{\rm p}_{\rm e2}$-$R_{\rm e}$ and $M^{\rm p}_{\rm e2}$-$\sigma_{\rm e2}$ correlations tend to have steeper total density profiles (i.e. higher values of γ'), while systems with higher values of $c_{\rm e2}$ have shallower total density profiles.

5.3. *Mass dependence of $R_{\rm e}$, $\sigma_{\rm e2}$ and $c_{\rm e2}$ for merger remnants*

The growth of galaxies by dry merging of smaller systems can be quantified by approximating the dependence of the structural parameters on mass with power-law functions: $R_{\rm e} \propto (M^{\rm p}_{\rm e2})^{\alpha_R}$, $\sigma_{\rm e2} \propto (M^{\rm p}_{\rm e2})^{\alpha_\sigma}$ and $c_{\rm e2} \propto (M^{\rm p}_{\rm e2})^{\alpha_c}$. For each step of a hierarchy the power-law indices are given by $\alpha_R \equiv \Delta \log R_{\rm e} / \Delta \log M^{\rm p}_{\rm e2}$, $\alpha_\sigma \equiv \Delta \log \sigma_{\rm e2} / \Delta \log M^{\rm p}_{\rm e2}$ and $\alpha_c \equiv \Delta \log c_{\rm e2} / \Delta \log M^{\rm p}_{\rm e2}$, where Δ indicates variation between the remnant and the progenitor [e.g. $\Delta \log R_{\rm e} = (\log R_{\rm e})_{\rm remnant} - (\log R_{\rm e})_{\rm progenitor}$]. We can obtain an estimate of the expected global effect of a general dry-merging hierarchy by considering the average values ($\langle \alpha_R \rangle = 0.85$, $\langle \alpha_\sigma \rangle = 0.06$, $\langle \alpha_c \rangle = 0.04$) and the associated standard deviations ($\delta\alpha_R = 0.17$, $\delta\alpha_\sigma = 0.08$, $\delta\alpha_c = 0.07$) of these values for our major and minor merging hierarchies (30 steps altogether). These values must be compared with the slope of the observed scaling laws (equations [3], [4] and [5]), which correspond to $\alpha_R = 0.63$, $\alpha_\sigma = 0.18$ and $\alpha_c = 0$, consistent with our statement that the MP is roughly preserved by dry mergers, but the mass–size and mass–velocity-dispersion relations are not.

Remarkably, the distributions of α_R, α_σ and α_c for our N-body experiments are characterized by a substantial scatter, which is quantified by the quoted values of the standard deviations. Such a broad distribution around the average slope is an additional problem for the dry-merging scenario, because it implies that dry mergers bf would introduce a lot of dispersion in the scaling relations. To quantify this, let us consider a population of galaxies, all with $M^{\rm p}_{\rm e2} = M_0$ and $R_{\rm e} = R_0$, that evolve through dry merging with an unspecified merging history made of both minor and major mergers (we are not assuming that these seed galaxies merge just among themselves): under the hypothesis that α_R is distributed normally, the merger remnants of mass $M^{\rm p}_{\rm e2} > M_0$ are expected to have $\log R_{\rm e}$ normally distributed with average $\langle \log R_{\rm e} \rangle = \log R_0 + \langle \alpha_R \rangle \log(M^{\rm p}_{\rm e2}/M_0)$ and standard deviation $\delta\alpha_R \log(M^{\rm p}_{\rm e2}/M_0)$. Thus, in this simple example, the predicted scatter in the $M^{\rm p}_{\rm e2} - R_{\rm e}$ relation at a given $M^{\rm p}_{\rm e2}$ increases for increasing $\delta\alpha_R$, and —for fixed $\delta\alpha_R$— increases for increasing $M^{\rm p}_{\rm e2}$, suggesting that a large enough mass growth by dry merging would produce a spread in $R_{\rm e}$ at given $M^{\rm p}_{\rm e2}$ inconsistent with the tight observed correlation. The importance of this effect can be appreciated by looking at the green shaded area in the central panel of Fig. 10, corresponding to the expected distribution, within 1 σ, of the merger remnants of a population of galaxies all with the same projected mass $M^{\rm p}_{\rm e2} = 10^{10.6} M_\odot$ (green vertical bar in the diagram), but now with a more realistic distribution of $R_{\rm e}$: we assume that $\log R_{\rm e}$ is normally distributed with average $\langle \log R_{\rm e} \rangle$ satisfying the observed $M^{\rm p}_{\rm e2}$-$R_{\rm e}$ correlation (equation [4]) and standard deviation equal to its intrinsic scatter (0.048 dex). Similar considerations apply to $c_{\rm e2}$ and $\sigma_{\rm e2}$ (green shaded areas in the top and bottom panels of Fig. 10). It is apparent that the scatter in $R_{\rm e}$ and $\sigma_{\rm e2}$ for the remnant population rapidly increases with mass above the observed scatter, while the effect is weaker in the $M^{\rm p}_{\rm e2}$-$c_{\rm e2}$ plane. The exact shapes of the green shaded areas depend on the set of merging

hierarchies considered. For instance, in the $M^{\rm p}_{\rm e2}$-$R_{\rm e}$, we find a weaker deviation from the observed correlation if we consider only model-D hierarchies, and a stronger deviation if we consider only minor-merging hierarchies (as a consequence of the specific behavior of these models; see § 5.2): in any case regions of the diagrams out of the observed strip are quickly populated.

Summarizing, we showed that the lensing mass–size and mass–velocity-dispersion relations are effectively destroyed by dry mergers, which produce systems with too large half-light radii and too low velocity dispersions, and introduce substantial scatter in $R_{\rm e}$ and $\sigma_{\rm e2}$ at given mass. We conclude that *present-day early-type galaxies did not form by dry merging of high-z early-type galaxies obeying the local ($z=0$) lensing scaling relations.*

6. DRY MERGERS AND REDSHIFT EVOLUTION OF EARLY-TYPE GALAXIES

In the previous section we explored the effect of dry mergers on galaxies lying on the lensing scaling relations observed locally. However, higher-z early-type galaxies must not necessarily obey the $z=0$ lensing scaling laws. In fact, though the lensing scaling relations at higher redshift are not available, measures of the effective radii and the stellar masses of high-redshift ($z\gtrsim 1-2$) early-type galaxies suggest that these objects may be remarkably more compact than their local counterparts (e.g., Daddi et al. 2005; Trujillo et al. 2006; Zirm et al. 2007; Cimatti et al. 2008; van Dokkum et al. 2008; van der Wel et al. 2008). As shown by our current results, as well as previous work (Nipoti, Londrillo & Ciotti 2003a; Boylan-Kolchin, Ma & Quataert 2006), dry merging has the effect of making galaxies less compact, so it has been proposed that evolution of early-type galaxies through such a mechanism might be consistent with the recent observational finding that higher-z galaxies are more compact (e.g., Khochfar & Silk 2006; Hopkins et al. 2009; van der Wel et al. 2009). Even allowing for the possibility that the candidate dry-merging progenitors of present-day early-type galaxies do not obey the local lensing scaling laws, the tightness of these correlations can be used to constrain the contribution of dry mergers in the assembly history of early-type galaxies.

For this purpose it is useful to consider the following question: under the hypothesis that local early-type galaxies (satisfying the lensing scaling laws) formed by dry merging, what are the expected properties of their (high-redshift) progenitors? To address this question we assume that the remnants of the last steps of all our simulated merging hierarchies satisfy the local $M^{\rm p}_{\rm e2}-R_{\rm e}$ relation. We then fix $\tilde{M}_*=10^{11}M_\odot$, and we choose a different value of $\tilde{r}_*$ for each hierarchy (in all cases smaller than the values of $\tilde{r}_*$ adopted in § 5), so $M^{\rm p}_{\rm e2}$, $R_{\rm e}$ and $\sigma_{\rm e2}$ are given in physical units for all models. The location of the models with respect to the observed lensing correlations is shown in Fig. 11: the most massive systems lie (by construction) on the observed $M^{\rm p}_{\rm e2}-R_{\rm e}$ relation (upper panel) and approximately also on the $M^{\rm p}_{\rm e2}-\sigma_{\rm e2}$ relation (lower panel), consistent with the fact that $c_{\rm e2}$ is not significantly affected by dry merging; less massive systems lie systematically below the $M^{\rm p}_{\rm e2}-R_{\rm e}$ relation and above the $M^{\rm p}_{\rm e2}-\sigma_{\rm e2}$ relation. In this picture the lowest-mass systems in the diagrams in Fig. 11 (those with $\log M^{\rm p}_{\rm e2}/M_\odot\lesssim 10.7$, all having by construction $M_*=10^{11}M_\odot$) would represent the high-z progenitors of local ellipticals. Given the idealized nature of our experiments, which are not set in a full cosmological context, we cannot define precisely the redshift of these progenitors. However, a lower limit to their redshift can be obtained by noting that the time to complete our merging hierarchies is in the range $6-12$ Gyr, with median ~ 9 Gyr. A realistic merging hierarchy is expected to be a mixture of steps of the explored hierarchies, so we take as reference time the median, which is the look-back time to $z\sim 1.4$. Therefore, in the present context, our seed galaxy models should be compared with $z\gtrsim 1.4$ early-type galaxies with stellar mass $\sim 10^{11}M_\odot$. The diagrams in Fig. 11 show that the candidate progenitors are predicted to be compact, with effective radii up to a factor of ~ 2.5 smaller and velocity dispersions up to a factor of ~ 1.6 higher than local galaxies with similar mass, and are characterized by a significant spread in both $R_{\rm e}$ and $\sigma_{\rm e2}$. We recall that the candidate progenitors have values of $c_{\rm e2}$ consistent with those observed in present-day galaxies, because our seed galaxies lie on the MP by construction. Though one cannot assume a priori that high-z progenitors lie on the MP, this assumption is justified as far as we are assuming —as working hypothesis— that local early-type galaxies formed by dry merging, because we have shown that dry mergers tend to preserve the MP.

The average properties of the candidate progenitors are qualitatively consistent with those of $z\gtrsim 1.4$ early-type galaxies (see Cimatti et al. 2008; Cappellari et al. 2009), so one might be tempted to conclude that a dry-merging scenario is compatible with observations. This is not necessarily the case, because the tightness of the local relations must be reproduced as well. In fact, as we are going to show, the tightness of the local relations sets the strongest constraints on dry merging, requiring a remarkable degree of fine tuning of the mix of progenitors and types of interaction.

This can be seen from the example shown in Fig. 10, where we focus, without loss of generality, on local early-type galaxies with projected mass $M^{\rm p}_{\rm e2}=10^{11.6}M_\odot$ (red vertical bars in the diagrams), and we constrain the properties of their progenitors in a dry-merging scenario. We have seen in § 5.3 that progenitors of given $M^{\rm p}_{\rm e2}$, $\sigma_{\rm e2}$ and $R_{\rm e}$ would produce through dry merging a population of galaxies with a range of values of $\sigma_{\rm e2}$, $R_{\rm e}$ and $c_{\rm e2}$ for given mass, depending on the expected distributions of α_R, α_σ and α_c, which are constrained by our N-body simulations. Here we take the opposite approach and impose that our reference present-day galaxies with $M^{\rm p}_{\rm e2}=10^{11.6}M_\odot$ have $\log c_{\rm e2}$, $\log R_{\rm e}$ and $\log\sigma_{\rm e2}$ with average values and intrinsic scatter consistent with observations. This procedure delivers constraints on $M^{\rm p}_{\rm e2}$, $\sigma_{\rm e2}$, $R_{\rm e}$ and $c_{\rm e2}$ in the form of "allowed" regions in the diagrams of Fig. 10 (red shaded areas). For instance, let us focus on the $M^{\rm p}_{\rm e2}-R_{\rm e}$ plane (central panel): at a given mass $M^{\rm p}_{\rm e2}<10^{11.6}M_\odot$, the upper and lower limits of the red shaded areas bracket the distribution within 1σ of $\log R_{\rm e}$ of a normally distributed population of galaxies of mass $M^{\rm p}_{\rm e2}$ that can produce via dry merging our population of galaxies with lensing mass $10^{11.6}M_\odot$. The same considerations apply to the $M^{\rm p}_{\rm e2}$-$c_{\rm e2}$ and $M^{\rm p}_{\rm e2}$-$\sigma_{\rm e2}$ planes.

It is clear that the smaller the shaded area, the higher the fine tuning necessary to obtain the local distributions.

While the constraints in the c_{e2} plane are weak (because c_{e2} is roughly preserved by dry merging), those in the σ_{e2} and R_e plane are quite strong and indicate that an uncomfortable degree of fine tuning is required in a dry merging scenario. Note, in particular, that a growth in M^p_{e2} via dry merging by more than a factor of ~ 2 (and in size by more than a factor of ~ 1.8) is excluded (see the red shaded area in the M^p_{e2}-R_e plane). Though our results constrain the projected mass M^p_{e2} measured within $R_e/2$, the upper limits on the mass growth can be extended to the total mass, because in our simulations M^p_{e2} increases with dry merging faster than the total mass (integrated over the entire system; see § 5.2). Therefore, our results indicate that present-day, massive early-type galaxies did not assembled more than 50% of their total (dark plus luminous) mass through dry merging.

One important caveat is that the allowed amount of mass growth depends on $\langle\alpha_R\rangle$ and $\delta\alpha_R$, and thus on the considered merging histories. Our set of simulations is biased in favour of major mergers and our exploration of the orbital parameter space is limited, especially in the case of the more DM dominated (model D, $f_* = 0.02$) galaxies. For instance, if we consider only our minor-merger hierarchies the upper limit to the mass fraction goes down to $\sim 40\%$, while this figure is $\sim 60\%$ if we consider only model-D hierarchies. In any case, a certain amount of fine tuning is required. Larger sets of numerical experiments, based on more realistic merging histories, are needed to quantify whether the amount of fine tuning required is consistent with hierarchical growth in a cosmological context.

From Fig. 10 it is also apparent that even an increase in mass by a factor smaller than 2 requires a lot of fine tuning, in the sense that the progenitors must have tighter mass–size and mass–velocity-dispersion correlations than local galaxies. This cannot be excluded, because there is no information so far on the lensing scaling relations beyond the redshift range covered by the SLACS sample ($z \sim 0.2 - 0.3$).

7. CONCLUSIONS

We explored the effect of minor and major dry mergers on the lensing scaling relations of early-type galaxies. Our main findings can be summarized as follows. Major and minor dry mergers:

1. Preserve the nearly isothermal structure ($\rho_{tot} \propto r^{-2}$) of early-type galaxies, adding a scatter of $\sim 9\%$ to the logarithmic slope (for an increase in stellar mass of up to a factor of ~ 8), consistent with the observed value of $\sim$10%.

2. Do not change the ratio between total (lensing) mass M^p_{e2} and "virial" mass ($R_e\sigma^2_{e2}/2G$) more than the observed scatter of 0.057 dex. In other words, they move galaxies along the MP.

3. Move galaxies away from the observed correlations between total (lensing) mass and size or velocity dispersion. Specifically, dry mergers increase the radius more rapidly than the scaling relation with mass would predict, while they do not increase velocity dispersion rapidly enough.

4. Add substantial scatter in the lensing mass-size and mass–velocity-dispersion relations.

The first two findings indicate that two important properties of early-type galaxies —the isothermal total mass profile and the MP— are quite robust against dry merging. If these regular structural and kinematic properties are established —presumably at $z > 1$, in order to satisfy constraints on the old age of their stellar populations (e.g., Treu et al. 2005) and of the lack of evolution of the logarithmic slope of the total mass density profile (Koopmans et al. 2006; Koopmans et al. 2009)— further growth via dry merging would not spoil this structural and kinematic homology of early-type galaxies.

The third and fourth findings pose a significant problem for a scenario where early-type galaxies grow significantly in mass via dry mergers. The non-conservation of the mass–size and mass–velocity-dispersion relation shows that the progenitors of present day early-type galaxies cannot be obeying the same scaling relations. On average, they will have to be smaller in size for a given velocity dispersion or total mass, qualitatively in line with some recent observational results (van der Wel et al. 2008). However, and most importantly, dry mergers add substantial scatter to the scaling relations. A few random generations of dry mergers would be sufficient to produce a scatter much larger than observed. In particular, our results exclude that present-day massive early-type galaxies assembled more than $\sim 50\%$ of their total (luminous plus dark) mass and increased their size by more than a factor ~ 1.8 via dry merging. Quantitatively, the amount of dispersion introduced in the scaling laws by dry merging depends on the detailed properties of the merging history, such as DM content of the progenitors and mass-ratio and orbital parameters of the galaxy encounters. A high degree of fine tuning - where the properties of the progenitor correlate with the peculiarities of the mergers process – would be needed to reconcile dry mergers with the tight observed lensing scaling relations.

In the present work we considered only gas-free mergers, so our results do not apply if mergers occur in the presence of significant amounts of gas. It is well known that dissipative processes might help reconcile merging with the standard scaling relations (e.g. Robertson et al. 2006; Ciotti, Lanzoni & Volonteri 2007; Johansson, Naab, & Burkert 2009a), so it is reasonable that the same can happen for the lensing scaling relations. However, the role of wet (gas-rich) mergers in the formation of early-type galaxies, though not strongly constrained by the scaling relations, is limited by other considerations: if these systems experienced a significant amount of mergers in relatively recent times, most of these mergers must have been dry, because the old stellar populations of early-type galaxies (e.g. Thomas et al. 2005) are inconsistent with substantial recent star formation. It is also the case that in very massive galaxies most accreted cold gas is likely to be eliminated by evaporation from the hot interstellar medium before it can form stars (Nipoti & Binney 2007).

We emphasize that our constraints on the dry-merging history apply to massive early-type galaxies, of which the SLACS sample is representative, and are not in conflict with the hypothesis that exceptionally luminous, brightest cluster galaxies (BCGs) formed via multiple dissipationless mergers, the so-called galactic cannibalism scenario (Ostriker & Tremaine 1975; Hausman & Ostriker 1978). In fact, numerical simulations of dynamical-friction driven galactic cannibalism predict that brightest cluster galaxies must be more extended than expected from the extrapolation of the size-luminosity correlation of smaller galaxies (Nipoti et al. 2003b; Ruszkowski & Springel 2009), as observed (e.g., Oegerle & Hoessel 1991; Bernardi 2009). In this respect, it will be very interesting to perform a systematic exploration of the behavior of brightest cluster galaxies with respect to the lensing scaling relations explored here. Larger numbers of BCGs with lensing features and stellar kinematics than those currently available (e.g., Sand et al. 2008) are needed to carry out this study.

In conclusion, we can see three main ways to make progress and determine whether the tightness of the lensing scaling relations is fatal to the idea of substantial growth of normal (i.e. non-BCG) early-type galaxies by dry mergers. From a theoretical point of view, fully cosmological simulations are needed to correlate properties of the progenitors with the details of the merging process and verify whether the required extraordinary amount of fine tuning does indeed occur. Also, future studies need to incorporate stellar mass as a fundamental variable that can also be directly linked to observations. From an observational point of view, large and homogeneous samples of lenses at higher-z than SLACS are needed to determine how the lensing scaling relations evolve with redshift.

We are grateful to our friends and collaborators on the SLACS project (M.W. Auger, S.C. Burles, M. Barnabé, O. Czoske, R. Gavazzi, L.V.E. Koopmans, P.J. Marshall, L.A. Moustakas, S. Vegetti) for many stimulating scientific conversations, and for their fundamental role in putting together the dataset that inspired this work. C.N. is happy to thank B. Nipoti for helpful discussions. Support for the SLACS project (HST-GO programs #10174, #10587, #10886, #10494, #10798, #11202) was provided by NASA through a grant from the Space Telescope Science Institute, which is operated by the Association of Universities for Research in Astronomy, Inc., under NASA contract NAS 5-26555. T.T. acknowledges support from the NSF through CAREER award NSF-0642621, by the Sloan Foundation through a Sloan Research Fellowship, and by the Packard Foundation through a Packard Fellowship. Some of the numerical simulations were performed using the BCX system at CINECA, Bologna, with CPU time assigned under the INAF-CINECA agreement 2008-2010.

REFERENCES

Bell, E.F. et al., 2006, ApJ, 640, 241
Bender, R., Burstein, D., & Faber, S.M. 1992, ApJ, 399, 462
Bernardi, M. 2009, MNRAS, 395, 1491
Binney, J., & Tremaine, S. 1987, Galactic Dynamics, Princeton University Press, Princeton
Bolton, A.S., Burles, S., Koopmans, L.V.E., Treu, T., & Moustakas, L.A. 2006, ApJ, 638, 703
Bolton, A.S., Burles, S., Treu, T., Koopmans, L.V.E., & Moustakas, L.A. 2007, ApJ, 665, L105
Bolton, A.S. et al., 2008a, ApJ, 682, 964
Bolton, A.S. et al., 2008b, ApJ, 684, 248
Bower, R.G., Lucey, J.R., & Ellis, R.S. 1992, MNRAS, 254, 601
Boylan-Kolchin, M., Ma, C.-P., & Quataert, E. 2006, MNRAS, 369, 1081
Bundy, K., Treu, T., & Ellis, R.S. 2007, ApJ, 665, L5
Cappellari M., et al., 2009, arXiv, arXiv:0906.3648
Carlberg, R.G. 1986, ApJ, 310, 593
Cimatti, A. et al., 2008, A&A, 482, 21
Ciotti, L., & van Albada, T.S. 2001, ApJ, 552, L13
Ciotti, L., Lanzoni, B., & Volonteri, M. 2007, ApJ, 658, 65
Daddi, E. et al., 2005, ApJ, 626, 680
Dehnen, W. 1993, MNRAS, 265, 250
Dehnen, W. 2002, Journal of Computational Physics, 179, 27
Dehnen, W. 2005, MNRAS, 360, 892
Djorgovsky, S., & Davis, M. 1987, ApJ, 313, 59
Dressler, A., Faber, S.M., Burstein, D., Davies, R.L., Lynden-Bell, D., Terlevich, R.J., & Wegner, G. 1987, ApJ, 313, 37
El-Zant, A.A., Hoffman, Y., Primack, J., Combes, F., & Shlosman, I. 2004, ApJ, 607, L75
Faber, S.M. et al., 2007, ApJ, 665, 265
Faber, S.M., & Jackson, R.E. 1976, ApJ, 204, 668
Ferrarese, L., & Merritt, D., 2000 ApJ, 539, L9
Fulton, E., & Barnes, J.E. 2001, Ap&SS, 276, 851
Gavazzi, R. et al., 2007, ApJ, 667, 176
Gebhardt, K. et al., 2000, ApJ, 539, L13
González-García, A.C., & van Albada, T.S. 2003, MNRAS, 342, L36
Häring, N., & Rix, H.-W. 2004, ApJ, 604, L89
Hausman, M.A., & Ostriker, J.P. 1978, ApJ, 224, 320
Hernquist, L. 1990, ApJ, 356, 359
Hopkins, P.F., Hernquist, L., Cox, T.J., Keres, D., & Wuyts, S. 2009, ApJ, 691, 1424
Jaffe, W. 1983, MNRAS, 202, 995
Johansson, P.H., Naab, T., & Burkert, A. 2009a, ApJ, 690, 802
Johansson, P.H., Naab, T., & Ostriker, J.P. 2009b, ApJ, 697, L38
Kazantzidis, S., et al. 2005, ApJ, 623, L67
Kazantzidis, S., Zentner, A.R., & Kravtsov, A.V. 2006, ApJ, 641, 647
Khochfar, S., & Burkert, A. 2003, ApJ, 597, L117
Khochfar, S., & Silk, J. 2006, ApJ, 648, L21
Koopmans, L.V.E., Treu, T., Bolton, A.S., Burles, S., & Moustakas, L.A. 2006, ApJ, 649, 599
Koopmans, L.V.E., Bolton, A., Treu, T., Czoske, O., Auger, M., Barnabe, M., Vegetti, S., Gavazzi, R., Moustakas, L., & Burles, S. 2009, ApJL, submitted
Kormendy, J. 1977, ApJ, 218, 333
Londrillo, P., Nipoti, C., & Ciotti, L. 2003, In "Computational astrophysics in Italy: methods and tools", Roberto Capuzzo-Dolcetta ed., Mem. S.A.It. Supplement, vol. 1, p. 18
Mandelbaum, R., Seljak, U., Kauffmann, G., Hirata, C.M., & Brinkmann, J. 2006, MNRAS, 368, 715
Marconi, A., & Hunt, L.K. 2003, ApJ, 589, L21
Merritt, D. 1985, AJ, 90, 102
Naab, T., Khochfar, S., & Burkert, A. 2006, ApJ, 636, L81
Naab, T., Johansson, P.H., Ostriker, J.P., & Efstathiou, G. 2007, ApJ, 658, 710
Naab, T., Johansson, P.H., & Ostriker, J.P. 2009, arXiv, arXiv:0903.1636
Navarro, J.F., Frenk, C.S., & White, S.D.M. 1996, ApJ, 462, 563 (NFW)
Nipoti, C., Londrillo, P., & Ciotti, L. 2002, MNRAS, 332, 901
Nipoti, C., Londrillo, P., & Ciotti, L. 2003a, MNRAS, 342, 501
Nipoti, C., Stiavelli, M., Ciotti, L., Treu, T., & Rosati P., 2003b, MNRAS, 344, 748
Nipoti, C., Treu, T., Ciotti, L., & Stiavelli, M. 2004, MNRAS, 355, 1119
Nipoti, C., Londrillo, P., & Ciotti, L. 2006, MNRAS, 370, 681
Nipoti, C., & Binney, J. 2007, MNRAS, 382, 1481

TABLE 1
SEED GALAXY MODELS.

Id	Model	$r_{\rm a}/\tilde{r}_*$	C_{200}	ξ	$M_{\rm dm}/\tilde{M}_*$	$N_{\rm tot}/10^5$	γ'
A5	A	1.4	7	7.8	10	11	2.02
A1	A	1.4	7	7.8	10	2.2	2.02
B5	B	∞	7	7.8	10	11	2.02
C5	C	0.7	7	7.8	10	11	2.02
D1	D	1.0	8	11.6	49	10	2.00

NOTE. — Id: name of the N-body realization. Model: name of the seed galaxy model. $r_{\rm a}$: anisotropy radius. C_{200}: NFW concentration. $\xi = r_{\rm s}/R_{\rm e}$. $M_{\rm dm}$: total dark-matter mass. $\tilde{M}_*$: total stellar mass. $N_{\rm tot}$: total number of particles in the N-body model (stellar and dark matter particles have the same mass). γ': logarithmic slope of the best-fit power-law total density profile ($\rho_{\rm tot} \propto r^{-\gamma'}$) over the radial range $0.1 \leq r/R_{\rm e} \leq 1$.

Nipoti, C., Treu, T., & Bolton, A.S. 2008, MNRAS, 390, 349
Oegerle, W.R., & Hoessel, J.G. 1991, ApJ, 375, 150
Osipkov, L.P. 1979, Soviet Astron. Lett., 5, 42
Ostriker, J.P. 1980, ComAp, 8, 177
Ostriker, J.P., & Tremaine, S.D. 1975, ApJ, 202, L13
Pipino, A., & Matteucci, F. 2008, A&A, 486, 763
Renzini, A. 2006, ARA&A, 44, 141
Romano-Díaz, E., Shlosman, I., Hoffman, Y., & Heller, C. 2008, ApJ, 685, L105
Robertson, B., Cox, T.J., Hernquist, L., Franx, M., Hopkins, P.F., Martini, P., & Springel, V. 2006, ApJ, 641, 21
Ruszkowski M., Springel V., 2009, ApJ, 696, 1094
Sand, D.J., Treu, T., Ellis, R.S., Smith, G.P., & Kneib, J.-P. 2008, ApJ, 674, 711
Scarlata, C., et al. 2007, ApJS, 172, 494
Thomas, D., Maraston, C., Bender, R., & Mendes de Oliveira, C. 2005, ApJ, 621, 673
Trager, S.C., Faber, S.M., Worthey G., & González, J.J. 2000, AJ, 120, 165
Tremaine, S., Richstone, D.O., Yong-Ik, B., Dressler, A., Faber, S.M., Grillmair, C., Kormendy, J., & Laurer, T.R. 1994, AJ, 107, 634
Treu, T., Ellis, R.S., Liao, T.X., van Dokkum, P.G., Tozzi, P., Coil, A., Newman, J., Cooper, M.C., & Davis, M. 2005, ApJ, 633, 174
Treu, T., Koopmans, L.V.E., Bolton, A.S., Burles, S., & Moustakas, L.A. 2006, ApJ, 640, 662
Treu, T., Gavazzi, R., Gorecki, A., Marshall, P.J., Koopmans, L.V.E., Bolton, A.S., Moustakas, L.A., & Burles, S. 2009, ApJ, 690, 670
Trujillo, I., et al. 2006, ApJ, 650, 18
van der Wel, A., Holden, B.P., Zirm, A.W., Franx, M., Rettura, A., Illingworth, G.D., & Ford, H.C. 2008, ApJ, 688, 48
van der Wel, A., Bell, E.F., van den Bosch, F.C., Gallazzi, A., & Rix, H.-W. 2009, arXiv, arXiv:0903.4857
van Dokkum, P.G. 2005, AJ, 130, 2647
van Dokkum, P.G., Franx, M., Fabricant, D., Kelson, D.D., & Illingworth, G.D. 1999, ApJ, 520, L95
van Dokkum, P.G., et al. 2008, ApJ, 677, L5
Zirm, A.W., et al. 2007, ApJ, 656, 66

TABLE 2
PARAMETERS OF THE SIMULATIONS AND PROPERTIES OF THE END-PRODUCTS.

Id	Prog.	$\hat{E}$	$\hat{L}$	d_0	$v_0^{\parallel}$	$v_0^{\perp}$	$M_{*,\rm fin}$	$M_{\rm dm,fin}$	$\sigma_{\rm v}$	$r_{\rm M,tot}$	γ'
2A5ph	A5	0	0	140	0.560	0	1.99	18.66	0.493	40.04	2.06
2A5po	A5	0	1.78	140	0.542	0.140	1.99	18.41	0.491	41.21	2.16
2B5ph	B5	0	0	140	0.560	0	1.99	18.99	0.486	41.22	2.08
2C5ph	C5	0	0	140	0.560	0	1.99	19.03	0.495	39.23	2.02
2A1ph	A1	0	0	140	0.560	0	1.99	19.01	0.490	40.28	2.08
2A1po	A1	0	1.78	140	0.542	0.140	1.99	18.76	0.492	41.17	2.18
2A1eh	A1	-0.83	0	140	0.336	0	2.00	19.73	0.525	33.77	2.06
2A1eo	A1	-0.83	1.78	140	0.305	0.140	2.00	19.62	0.535	35.65	2.27
2A1hh	A1	0.83	0	140	0.716	0	1.98	17.91	0.459	42.69	2.13
2A1ho	A1	0.83	1.78	140	0.702	0.140	1.98	17.59	0.467	40.98	2.27
2D1ph	D1	0	0	240	0.910	0	1.99	92.66	0.746	72.79	1.82
2D1po	D1	0	1.78	240	0.886	0.218	1.99	92.55	0.743	75.88	1.92
4A1ph	2A1ph	0	0	280	0.548	0	3.95	36.52	0.526	69.49	1.95
4A1po	2A1po	0	1.78	280	0.528	0.130	3.95	35.28	0.530	85.17	2.16
4A1eh	2A1eh	-0.83	0	280	0.286	0	3.99	38.72	0.613	55.72	1.99
4A1eo	2A1eo	-0.83	1.78	280	0.238	0.120	3.99	38.38	0.583	63.14	2.23
4A1hh	2A1hh	0.83	0	280	0.678	0	3.90	32.10	0.473	90.19	1.98
4A1ho	2A1ho	0.83	1.78	280	0.668	0.122	3.90	29.51	0.481	87.52	2.24
4D1ph	2D1h	0	0	480	0.888	0	3.89	176.93	0.803	134.09	1.70
4D1po	2D1o	0	1.78	480	0.864	0.208	3.98	175.23	0.804	152.65	1.77
8A1ph	4A1ph	0	0	560	0.538	0	7.85	70.78	0.550	160.47	1.95
8A1po	4A1po	0	1.78	560	0.509	0.144	7.82	65.83	0.528	201.62	2.18
8A1eh	4A1eh	-0.83	0	560	0.066	0	7.95	76.15	0.679	84.12	1.84
8A1eo	4A1eo	-0.83	1.78	560	0.086	0.114	7.95	75.46	0.660	106.01	2.16
8A1hh	4A1hh	0.83	0	560	0.666	0	7.63	55.91	0.490	169.73	1.96
8A1ho	4A1ho	0.76	0.80	560	0.640	0.060	7.60	50.44	0.491	184.16	2.13
2A5m10x	A5	-	-	-	-	-	1.86	15.81	0.587	22.64	2.11
2A1m10x	A1	-	-	-	-	-	1.86	16.09	0.585	23.02	2.11
2A1m10y	A1	-	-	-	-	-	1.86	15.66	0.554	25.28	1.84
2A1m5	A1	-	-	-	-	-	1.76	14.67	0.550	23.87	2.03
2D1m10	D1	-	-	-	-	-	1.69	73.13	0.896	37.74	1.65
4A1m10x	2A1m10x	-	-	-	-	-	3.21	26.99	0.642	32.01	1.99
4A1m10y	2A1m10y	-	-	-	-	-	3.61	30.18	0.557	48.47	1.94
4A1m5	2A1m5	-	-	-	-	-	3.29	26.69	0.597	38.83	2.10
4D1m10	2D1m10	-	-	-	-	-	3.07	119.29	0.993	50.07	1.66

NOTE. — Id: name of the run and of the corresponding end-product. Prog.: name of the progenitor. $\hat{E}$: dimensionless orbital energy. $\hat{L}$: dimensionless orbital angular momentum modulus. d_0: initial separation. $v_0^{\parallel} \equiv \mathbf{v}_0 \cdot \mathbf{d}_0/d_0$: parallel component of the initial relative velocity. $v_0^{\perp} \equiv ||\mathbf{v}_0 \times \mathbf{d}_0||/d_0$: orthogonal component of the initial relative velocity. $M_{*,\rm fin}$: final stellar mass. $M_{\rm dm,fin}$: final dark matter mass. $\sigma_{\rm v}$: virial velocity dispersion of the end-product. $r_{\rm M,tot}$: circularized half-mass radius of the total density distribution of the end-product. γ': logarithmic slope of the best-fit power-law total density profile ($\rho_{\rm tot} \propto r^{-\gamma'}$) over the radial range $0.1 \leq r/R_{\rm e} \leq 1$. Masses, lengths and velocities are in units of $\tilde{M}_*$, $\tilde{r}_*$ and $\tilde{v}_*$, respectively. The parameters $\hat{E}$, $\hat{L}$, d_0, $v_0^{\parallel}$ and $v_0^{\perp}$ are defined only for binary major-merging simulations.